processes

MDPI

Article

Heteroatom-Doped Carbon-Based Catalysts Synthesized through a "Cook-Off" Process for Oxygen Reduction Reaction

Ruiquan Zhang [1], Qiongyu Liu [2], Ming Wan [1], Zhenhua Yao [1,*] and Maocong Hu [1,*]

[1] School of Optoelectronic Materials & Technology, Jianghan University, Wuhan 430056, China; ruiquan.zhang@stu.jhun.edu.cn (R.Z.); wanming@jhun.edu.cn (M.W.)
[2] School of Environment and Health, Jianghan University, Wuhan 430056, China; qiongyuliu@163.com
* Correspondence: zhenhua.yao@jhun.edu.cn (Z.Y.); maocong.hu@jhun.edu.cn (M.H.); Tel.: +86-27-8439-2310 (M.H.)

Abstract: The development of efficient and low-cost non-metallic catalysts is of great significance for the oxygen reduction reaction (ORR) in fuel cells. Heteroatom-doped carbon-based catalysts are one of the popular candidates, although their preparation method is still under exploration. In this work, single (CS)-, double (NCS)-, and triple (NBCS)-heteroatom-doped carbon-based catalysts were successfully prepared by a "cook-off" process. The morphology, elemental composition, and bonding structure of the catalysts were investigated by SEM, TEM, Raman spectra, BET, and XPS. ORR catalytic performance measurements suggested an activity trend of CS < NCS < NBCS, and NBCS demonstrated better methanol resistance and slightly higher stability than the commercial Pt/C catalyst, as evaluated with both rotating disk electrode (RDE) and rotating ring-disk electrode (RRDE) systems. The mechanism for the promoted performance was also proposed based on the conductivity of the catalysts. In this paper, the heteroatoms N, B, and S were co-doped into activated carbon using a simple, fast, and efficient preparation method with high electrical conductivity and also increased active sites, showing high electrocatalytic activity and good stability. This work provides a new approach to preparing highly active non-Pt catalysts for oxygen reduction reactions.

Keywords: metal-free catalyst; "cook-off" process; heteroatom doping; oxygen reduction reaction

Citation: Zhang, R.; Liu, Q.; Wan, M.; Yao, Z.; Hu, M. Heteroatom-Doped Carbon-Based Catalysts Synthesized through a "Cook-Off" Process for Oxygen Reduction Reaction. *Processes* **2024**, *12*, 264. https://doi.org/10.3390/pr12020264

Academic Editor: Alexander S. Novikov

Received: 23 December 2023
Revised: 23 January 2024
Accepted: 24 January 2024
Published: 25 January 2024

1. Introduction

With the increase in global energy consumption and concerns about environmental pollution, the demand for sustainable, renewable, clean, and environmentally friendly energy has become urgent. The fuel cell is an efficient and clean energy device that directly converts chemical energy into electrical energy through chemical reactions, which is one of the most promising technical approaches to solving energy and environmental problems and has attracted the attention of the community. The chemical reactions associated with fuel cell devices consist of an anode reaction and a cathode reaction while the cathodic reaction is kinetically much more sluggish than the anodic one [1,2]. Therefore, catalysts with the ability to improve ORR kinetics are required to enhance the efficiency of fuel cells. Currently, the commercially available precious metal platinum and its alloy catalysts show excellent ORR activity [3]. However, its expensive price, limited reserves, as well as poor durability are the concerns regarding their large-scale application. Therefore, new types of catalysts with cost-effective and durable properties are under development aiming to replace Pt and Pt-based alloy catalysts [4]. As one of the popular candidates, non-metallic carbon-based catalysts have been widely investigated and attracted considerable attention since it was first reported in 2009 that nitrogen-doped carbon nanotubes were active for ORRs [5]. Generally, based on the number of doping elements, heteroatom-doped carbon materials could be roughly categorized into single heteroatom doping (e.g., N-, S-, B-, P-, F-, etc.) [6–12] and multi-heteroatom doping (e.g., N, S-; N, B-; N, P, S-; N, B, P-; N, B, F-; N, B, S-; etc.), respectively [13–20]. Park et al. reported the synthesis of sulfur-doped

graphene by a heat treatment method. The limiting current density increases with higher sulfur content and S acts to increase the catalytic activity [21]. Hu et al. reported unique, two-dimensional (2D) N, S co-doped graphite flakes with a hierarchical structure of three-dimensional pores on the surface of the catalyst, which provided abundant active sites and exhibited good catalytic performance [22]. Li et al. reported N/B/S-doped graphitized-coated Fe composites, and through this simple and effective strategy, the catalyst attained a multistage porous structure with good mass transfer properties, high doping levels for N, S, and B, and significant ORR activity [16]. It is widely accepted that atomic size and electronegativity differences between heteroatoms and carbon atoms could effectively change the intrinsic electronic properties of the carbon substrate, which further generates active sites and improves catalytic performance [23].

A multitude of methods have been reported for doping heteroatoms into carbon materials such as chemical vapor deposition (CVD), sol–gel, ball milling, and hydrothermal methods [24,25]. Theoretically, perfect doped structures could be harvested with the CVD method, but the slow deposition rate, high production cost, long reaction time, and potentially hazardous substances produced during the process limit its application [26]. Being time-consuming was considered as the obvious drawback of sol–gel method, although it was widely used [27]. The ball milling method is famous for its simplicity while the inevitable introduction of impurities during the process may make the investigation more complicated [28]. The hydrothermal method is well established for doped material preparation while operation safety and incomplete doping are issues to be solved [29]. Therefore, methods other than those described above are still required to synthesize superior-performance heteroatom-doped catalysts.

In this work, we reported a novel "cook-off" process to prepare both single heteroatom (S-) and multi-heteroatom (N, S- and N, B, S-)-doped ORR catalysts. The reactants were rapidly heated to a high temperature so that the combustion occurred in a short time, which led to the release of a large amount of heat. As a result, the system reached extremely high temperatures. It further resulted in the generation of a certain degree of graphitization on the surface of the carbon substrate, which improved the electrical conductivity of obtained catalysts [30]. The morphology, elemental composition, and bonding structure were investigated by scanning electron microscopy (SEM), transmission electron microscopy (TEM), Raman spectra (Raman), Brunauer–Emmett–Teller specific surface area (BET), and X-ray photoelectron spectroscopy (XPS). A systematic investigation of ORR catalytic performance, including activity and stability, was carried out by employing LSV, K-L plots, Tafel plots, methanol resistance, and long-term operation. The mechanism for the promoted performance was also proposed based on the conductivity measurement. This work provides a new perspective on preparing superior-performance heteroatom-doped carbon-based ORR catalysts.

2. Experimental

2.1. Preparation

Three heteroatom-doped carbon-based catalysts were prepared with activated carbon as a carbon source, sublimated sulfur as a sulfur source, urea as a nitrogen source, and boric acid as a boron source, while potassium nitrate was employed for deflagration purposes. Based on the chemicals used and their mass ratio, the sublimation sulfur-doped activated carbon was named CS (C:S = 0.15:0.1), the urea and sublimation sulfur co-doped activated carbon was named NCS (N:C:S = 0.6:0.15:0.1), and the urea, sublimation sulfur, and boric acid co-doped activated carbon was named NBCS (N:B:C:S = 0.6:0.1:0.15:0.1). Typical amounts of the raw materials are listed in Table S1, while the preparation procedure is shown in Figure 1. The crucible with pre-ground raw materials inside was quickly put into a melting furnace, which was preheated to 700 °C. A slight smoke began to come out after about 2 min, and it became bigger as the fire spouted out of the furnace after about 5 min. The power was then turned off, and the crucible was immediately taken out to cool down to a normal temperature. The residual material was then collected from the crucible, which

was further washed five times using deionized water with a vacuum filtration system. Finally, the desired sample was obtained by drying at 60 °C for 10 h.

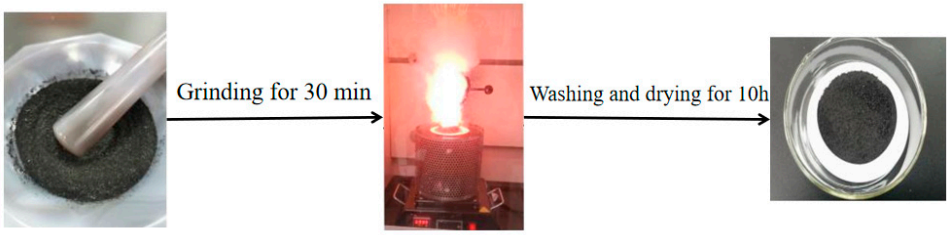

Figure 1. Preparation of heteroatom-doped carbon-based catalysts with a "cook-off" process.

2.2. Characterizations

X-ray photoelectron spectrometry (XPS) was used to establish the apparent constituents of the compounds and the form in which they existed based on binding energies (model AXIS Supra+, Shimadzu, Kyoto, Japan). The extent of graphitization and disorder on the surface of the carbon material was analyzed using a Raman microscope (inVia™ type, Renishaw, Wotton-under-Edge, UK). A surface area and porosity analyzer (BET) were used to perform isothermal adsorption and desorption analysis using the principle of gas adsorption to determine the specific area and pore size distribution of the sample (model ASAP020, MICROMERITICS). SEM and TEM were used to observe the morphology and microstructure of the catalysts using models SU8010 and HT7700, Hitachi, Tokyo, Japan, respectively. The conductivity of the catalysts was detected with a four-probe powder resistivity tester (model ST2722, Suzhou Jingge Electronic Co., Ltd., Suzhou, China).

2.3. Electrochemical Measurements

A three-electrode system was used to characterize the catalytic performance on a Shanghai Chenhua CHI760E electrochemical workstation. Ag/AgCl was employed as the reference electrode (RE), a platinum wire coil was the counter electrode (CE), and the working electrode (WE) was a polished rotating disk electrode (RDE, ALS Co., Ltd., Tokyo, Japan) with dispersed catalysts on it. The dispersed catalyst was prepared by adding 20 mg of catalyst to a mixture of 2 mL of DMF and 50 µL of Nafion (5 wt%). It was then ultrasonically dispersed for 30 min to form a homogeneously dispersed solution, while 3 µL of this solution was pipetted onto the RDE for ORR testing. The electrolyte (0.1 M KOH) was saturated with oxygen while the data were collected from −0.9 V to 0.2 V using linear scanning voltammetry (LSV). The scanning rate was set as 10 mV s^{-1} while the rotation speed of the RDE was 400–2500 rpm. An LSV test was also performed under the saturating condition of nitrogen, while the final current was obtained by subtracting the oxygen data from the nitrogen data, which were further fitted for kinetic analysis. Based on the experimentally determined boundary conditions, the Levich Equation (1) and the Koutecky–Levich Equation (2) were employed for the kinetic analysis, and the details of both equations are reported in the literature [31]:

$$B = 0.62nFC_{O_2}\left(D_{O_2}\right)^{\frac{2}{3}}v^{\frac{-1}{6}} \quad (1)$$

$$\frac{1}{J} = \frac{1}{J_K} + \frac{1}{J_L} = \frac{1}{J_K} + \frac{1}{B\omega^{\frac{1}{2}}} \quad (2)$$

In addition, rotating ring-disk electrode (RRDE, ALS Co., Ltd., Tokyo, Japan) measurements were also performed with a scan rate was 10 mV s^{-1} and a ring electrode potential of 0.1 V. The yield of H_2O_2 and the number of transferred electrons (n) were calculated by Equations (3) and (4):

$$H_2O_2 = 200 \times \frac{\frac{I_{ring}}{N}}{I_{disk} + \frac{I_{ring}}{N}} \quad (3)$$

$$n = 4 \times \frac{I_{disk}}{I_{disk} + \frac{I_{ring}}{N}} \quad (4)$$

See the Supporting Information for the specific parameters.

The durability and methanol resistance of the catalyst were characterized using the timed-current method (i–t curve) at a stable voltage (−0.4 V) for 10,000 s to test its durability performance, and the methanol resistance was tested by adding 3 M CH_3OH to an oxygen-saturated electrolyte at a stable condition for 100 s of operation.

The Tafel slope is calculated from the LSV curve measured by ORR. The formula for the Tafel slope is given below:

$$\eta = a + blog|J| \quad (5)$$

η denotes overpotential; a denotes the Tafel constant; b denotes the Tafel slope; J denotes measured current density.

3. Results and Discussion

3.1. Characterizations of Heteroatom-Doped Carbon-Based Catalysts

The morphologies of the prepared catalysts (NBCS, NCS, and CS) were characterized by SEM. NBCS demonstrated uniform surface distribution with particles of similar sizes, as shown in Figure 2a. It provided sufficient active sites, which made the oxygen molecules easy to adsorb and promoted the oxygen reduction reaction over NBCS. In addition, the homogeneous surface could also provide a platform for fast electron transport, resulting in the enhancement of the electrical conductivity of NBCS, which would benefit the increase in the reaction rate [32]. Compared with the case of NBCS, the uneven surface distribution of NCS in Figure 2b and CS in Figure 2c, with obvious particle aggregation as well as holes produced the during "cook-off" process, was observed. This may lead to the obstruction of electron transport which further decreases electron conductivity and affects the electron conduction efficiency. Moreover, some active sites may be covered or destroyed due to the aggregation or holes, which may finally decrease the ORR reaction rate and catalytic activity. Since activated carbon is an amorphous carbon with no obvious ordered crystal structure, no useful information was collected with transmission electron microscopy (TEM), as indicated in Figure S1.

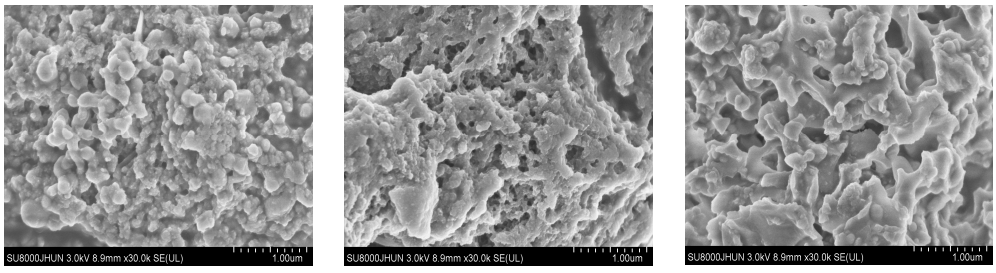

(**a**) (**b**) (**c**)

Figure 2. SEM images of (**a**) NBCS; (**b**) NCS; (**c**) CS.

Raman spectroscopy was further used to feature the heteroatom-doped carbon-based catalysts to study the level of internal defects and graphitization of the prepared samples. As demonstrated in Figure 3, two distinct characteristic peaks at positions near 1350 cm^{-1} (D peak) and 1580 cm^{-1} (G peak) were observed for all three samples [33,34]. The D peak represents the internal imperfection and disorder of the carbon material structure, while the G peak represents the degree of graphitization of the carbon material structure. Moreover, the strength (I_D/I_G) ratio of the D and G peaks represents the disorder in the structure of the carbon material. A larger ratio usually indicates a higher degree of defects in the material [35,36]. The intensity ratios (I_D/I_G) of the peaks of NBCS, NCS, and CS were determined to be 1.03, 0.94, and 0.97, respectively, which indicated that the high temperature generated instantaneously during the "cook-off" process increased the extent

of graphitization on the surface of the carbon materials, as in the cases of NCS and CS. However, the synergistic effect produced by ternary doping hindered graphitization as demonstrated by NBCS ($I_D/I_G > 1$) [37]. Therefore, it further broke the original carbon material structure and increased the internal defects and disorder, which may enhance the activity of NBCS for ORR [38]. In addition, the above results also show that the "cook-off" process ensures that the heteroatoms are doped while maintaining a certain degree of graphitization, which provides a new idea for the future development of a process that maintains both doping and a high level of graphitization at the same time. Raman data showed that NCS was the most graphitized, CS was the second most graphitized, and NBCS was the least graphitized, which is consistent with the data obtained by SEM. Scanning electron microscopy images show that NCS is highly crystalline, agglomerated, and graphitized, CS is the second most crystalline, and NBCS is the least crystalline with the largest degree of looseness.

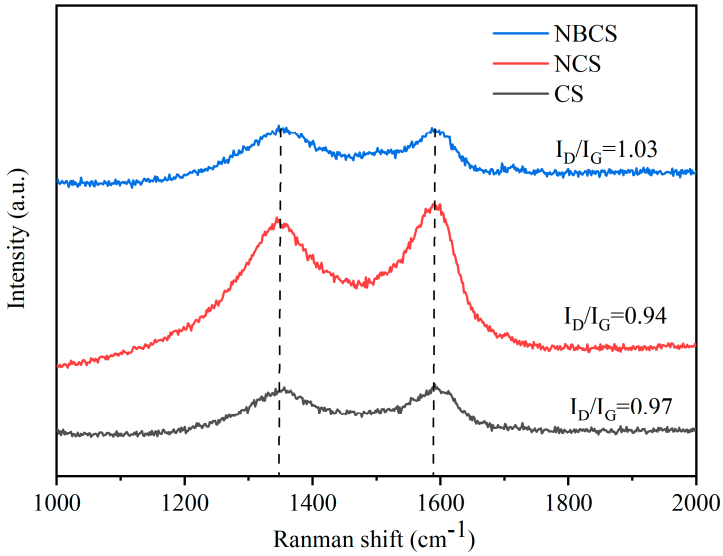

Figure 3. Raman spectra of NBCS, NCS, and CS.

The specific surface area and porous structure of the resulting catalysts were further characterized by N_2 adsorption/desorption measurements. As can be seen from Figure 4a, the adsorption isotherms and desorption isotherms of the three catalysts do not overlap and form hysteresis returns at different relative pressures, which are typical characteristics of type IV adsorption isotherms. The specific area of CS is 100.14 cm^2 g^{-1}, that of NCS is 280.08 cm^2 g^{-1}, and that of NBCS is 144.28 cm^2 g^{-1}. These data indicate that the reason for the larger specific surface area from single to double doping is that the heteroatoms are doped on the carbon material, which increases the specific surface area of the carbon material. On the other hand, triple doping has a larger specific surface area than single doping and a smaller one than double doping. This can be attributed to the fact that an excessive amount of heteroatoms blocked the pores of the activated carbon, resulting in a decrease in the specific surface area [39]. In addition, it can be seen from Figure 4b that there are many mesopores and macropores in the pore size distribution of NBCS, where mesopores are beneficial for generating more structural defects and transporting reaction intermediates, and macropores are beneficial for facilitating the mass transfer and increasing the mass transfer rate of the reaction [40]. The pore size distribution of CS and NCS is approximately the same as that of NBCS, as detailed in Figure 4b.

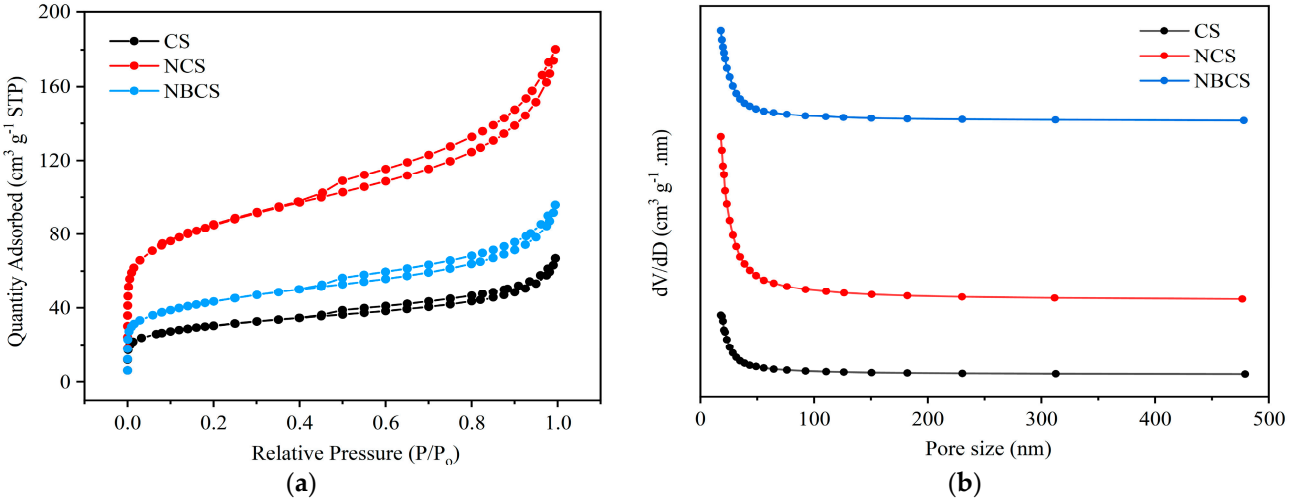

Figure 4. (**a**) N_2 adsorption–desorption isotherms of CS, NCS, NBCS; (**b**) BJH pore size distribution of CS, NCS, NBCS.

The elemental (N, B, C, S) composition and the corresponding chemical states of the prepared catalysts were identified using XPS, as shown in Figure 5. The full spectra and specific elemental composition contents of NBCS, NCS, and CS are depicted in Figure 5a and Table S2. Five characteristic peaks, S 2p, B 1s, C 1s, N 1s, and O 1s, located at 164 eV, 186 eV, 284.4 eV, 377 eV, and 533 eV, respectively, were observed, which suggested that the N, B, and S elements were successfully incorporated into the carbon matrix [41]. Moreover, the sulfur element (S) was contained in all three samples, even though the doping amounts were different (3.7, 2.3, and 1.7%, respectively), which may be due to the different formulations of raw materials used in NBCS, NCS, and CS, resulting in different levels of deflagration. The high-resolution O 1s spectrum of NBCS, NCS, and CS (Figure 4b) showed that C–O and C=O were observed in all three samples [42]. This can be ascribed to the large amount of oxygen generated from KNO_3 during the "cook-off" process, which reached an oxygen-rich state leading to the doping of the oxygen element into the carbon substrate under high-temperature conditions. B–O was also observed over NBCS, indicating the successful insertion of boron. Moreover, the obvious peak shift of both C–O and C=O was displayed for all three samples (Figure 5b), which indicated the different micro-environment of these two bonds in the three catalysts. This may be attributed to the different kinds of doping (i.e., single-, double-, and triple- doping). The high-resolution C 1s spectrum of NBCS, NCS, and CS (Figure 5c) clearly recorded C–C, C–O, C–S, C–N, and C–B [43,44], which further demonstrated that heteroatoms N, B, and S were doped into the carbon substrate. Moreover, the successful detection of O=C–O (π–π^*) demonstrated the presence of graphite structures in the prepared catalysts [45]. Figure 5d showed the high-resolution S 2p spectra of three catalysts, consisting of S-C (thiophene S), SO_x 2p 1/2, and SO_x 2p 3/2 (oxidized S) [46], and thiophene S is widely considered to have a positive effect on increasing ORR activity [47]. A peak shift was also observed in the bonding energy of these structures due to the different doping types. The high-resolution N 1s spectrum of NBCS and NCS (Figure 5e) demonstrated three characteristic nitrogen peaks: pyridinic N, pyrrolic N, and graphitic N [48,49]. Pyridinic N was reported as a donator to provide a p-electron to the π-system and further form a lone pair of electrons, leading to a neighboring carbon atom with high activity for ORR [50]. Graphitic N favors electron conduction, benefitting electron transfer and onset potentials as well as suppressing current density. Therefore, there is a need to balance these two types of N, which would be useful to improve the ORR electrocatalytic performance of N-doped carbon-based catalysts [51,52]. As listed in Table S2, a higher percentage of pyridinic N was observed in NBCS (0.258% of 0.6%) compared to that of NCS (1.289% of 3.4%), which definitely affected their ORR performance. The high-resolution B 1s spectrum of NBCS is illustrated in Figure 5f. It could be deconvoluted into two

characteristic peaks, BC_2O and BCO_2, respectively [53]. The B-N structure, which was not observed within NBCS, favors the maintenance of high N contents [54]. As a result, relatively low N was recorded in NBCS, as shown in Table S2. Moreover, due to the absence of B–N, boron would preferentially react with oxygen to form boron oxides, which further immobilize oxygen to prevent nitrogen fixation during the "cook-off" process. Therefore, the nitrogen content of NBCS is much lower than that of NCS.

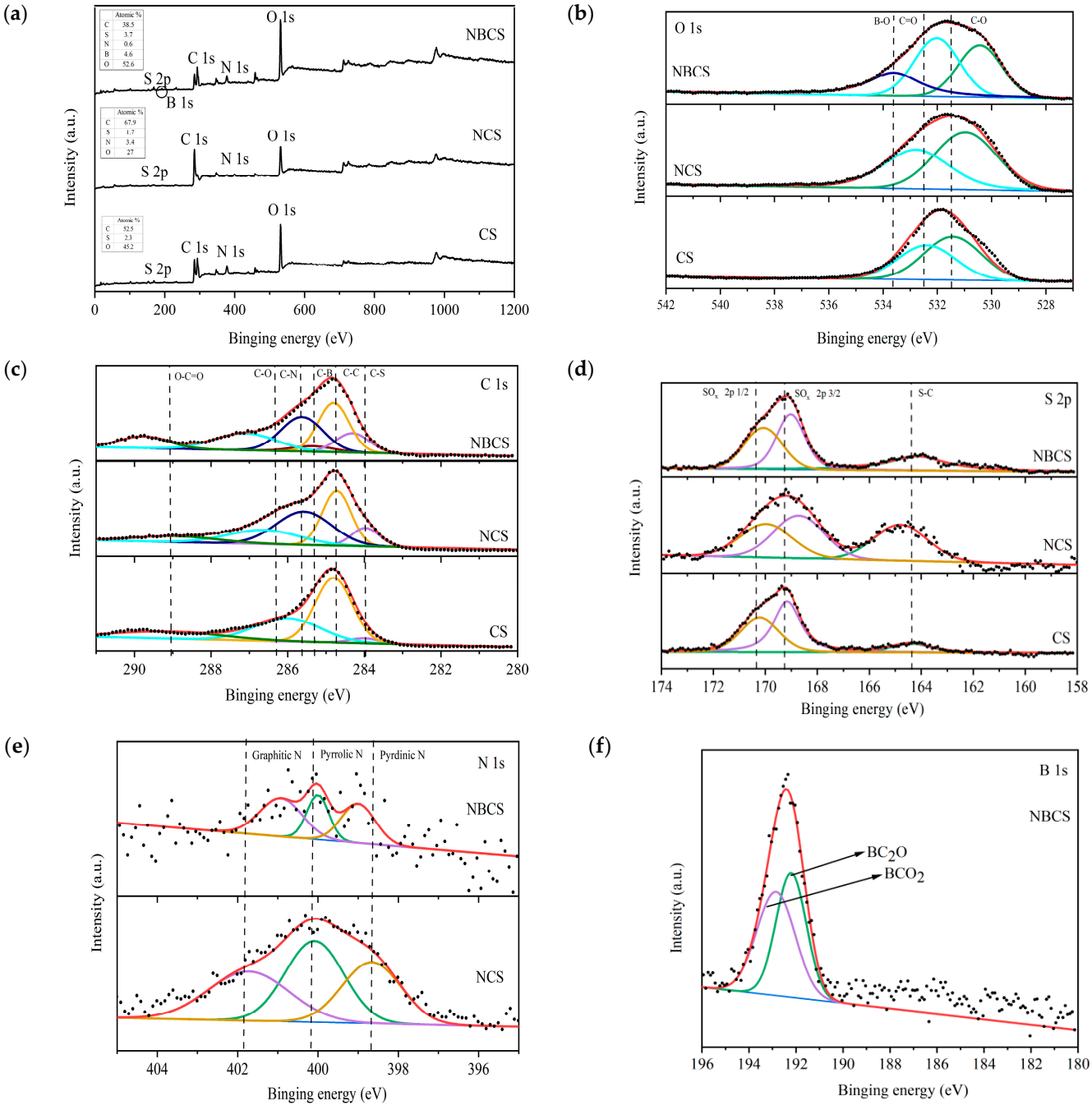

Figure 5. (**a**) XPS of NBCS, NCS, and CS; (**b**) O 1s of NBCS, NCS, and CS; (**c**) C 1s of NBCS, NCS, and CS; (**d**) S 2p of NBCS, NCS, and CS; (**e**) N 1s of NBCS and NCS; (**f**) B 1s of NBCS. The solid line in red is the sum of all the peak fittings while the curves in other colors represent elements with different valence state.

The best ORR catalytic performance of NBCS can be attributed to the structure benefitting the ORR. The homogeneous surface distribution of NBCS, as demonstrated in SEM,

accelerated the electron transfer rate. The degree of graphitization exhibited in NBCS, as shown in Raman spectra, improved the conductivity. The large specific surface area and abundant porous structure of NBCS as measured by BET provided it with more active sites, which promoted the mass transfer and accelerated the reaction kinetics. The high percentage of pyridinium N of NBCS as confirmed by XPS effectively modulated the electrocatalytic performance.

3.2. Catalytic Performance

The LSV curves of NBCS, NCS, CS, and Pt/C at 1600 rpm are demonstrated in Figure 6a, and the current densities of NBCS, NCS, and CS were −4.98, −4.71, and −3.94 mA cm^{-2}, with the trend of NBCS > NCS > CS. The loadings and initial potentials E_{onset} and half-wave potentials $E_{1/2}$ of the resulting catalysts are shown in Table 1. Moreover, the LSV at different rotational speeds (400–2500 rpm) of NBCS is shown in Figure 6b. The current density increased with increasing speed due to enhanced electrolyte diffusion [55,56]. A good linear relationship was achieved based on LSV obtained at different rotational speeds (see Figure 6c), indicating the presence of a first-order response to dissolved oxygen over NBCS [57–59]. The slopes of the fitting lines were further calculated using the K-L equation, while the numbers of electrons transferred (n) at different potentials during the reaction were then determined as listed in Figure 6c. The numbers were in the range of 3.82 to 3.96, a typical four-electron pathway. Similarly, the number of transferred electrons of Pt/C and NCS was calculated to be 3.93~3.99 and 3.88~3.97, respectively (Figure 6d), which indicated that both also predominantly went through a four-electron transfer process. However, the electron transfer number of CS was determined to be between 3.2 and 3.34, which is intermediate between the two-electron and four-electron oxygen reduction processes. This indicates that CS was involved in both two-electron and four-electron reactions. The Tafel slope can affect the rate and efficiency of a catalytic reaction. The smaller the Tafel slope is, the faster the reaction rate is and the higher the catalytic activity is [60]. The Tafel diagram of NBCS, NCS, CS, and Pt/C is shown in Figure 6e. The Tafel slope of NBCS (86.74 mV dec^{-1}) was lower than that of Pt/C (87.86 mV dec^{-1}), NCS (98.45 mV dec^{-1}), and CS (102.96 mV dec^{-1}), which further indicated that NBCS exhibited the fastest kinetics for ORR. The electrocatalytic performance of NBCS, NCS, CS, and Pt/C was further studied using the RRDE technique. The I_{ring} and I_{disk} of the catalysts at 1600 rpm were shown in Figure 6f, while H_2O_2 yield (%) and the number of transferred electrons (n) during the ORR process was calculated using Equations (3) and (4), as listed in Figure 6g. The number of transferred electrons for NBCS was 3.89 while H_2O_2 yield was 4.65%. The result (3.89) is consistent with the number of transferred electrons calculated by the K-L equation (3.82–3.96). This indicated that the electrocatalytic process with NBCS was dominated by four-electron transfer, with water as the main product and a small amount of hydrogen peroxide as a byproduct, which further suggested that NBCS was a good candidate for ORR [61]. NCS also demonstrated a four-electron pathway (3.93) while the amount of byproduct (6.22%) was higher than that of NBCS (4.65%). Byproducts accounted for around 14% in the case of CS, suggesting it is not suitable for ORR applications.

Methanol resistance was further measured by chronoamperometry (Figure 6h), and 3 M CH_3OH was introduced into oxygen-saturated 0.1 M KOH electrolyte. As expected, a dramatic decrease in current was observed on Pt/C (49.5%), as reported by the literature [62,63]. Interestingly, a slight change (3.3%) was recorded for NBCS, indicating its superior methanol resistance compared to Pt/C. Stability tests were carried out by using a timed-current methodology approach with a fixed potential at −0.4 V (Figure 6i). After a duration of 10,000 s, NBCS still maintained 93.89% of the initial current density, while that of Pt/C was 89.78%, indicating that NBCS showed slightly better stability than Pt/C. Based on the above electrochemical measurements and analysis including LSV, K-L plots, the number of transferred electrons, Tafel plots, H_2O_2 yields, methanol resistance, and stability tests, it can be concluded that the N, B, and S triple co-doped carbon-based catalyst (NBCS) prepared through the "cook-off" process showed comparable or better catalytic

performance for ORR as compared with commercial Pt/C. By recording the data related to heteroatom-doped carbon materials for ORR with Table S3, it can be concluded that the catalysts prepared in this work showed close performance with the literature.

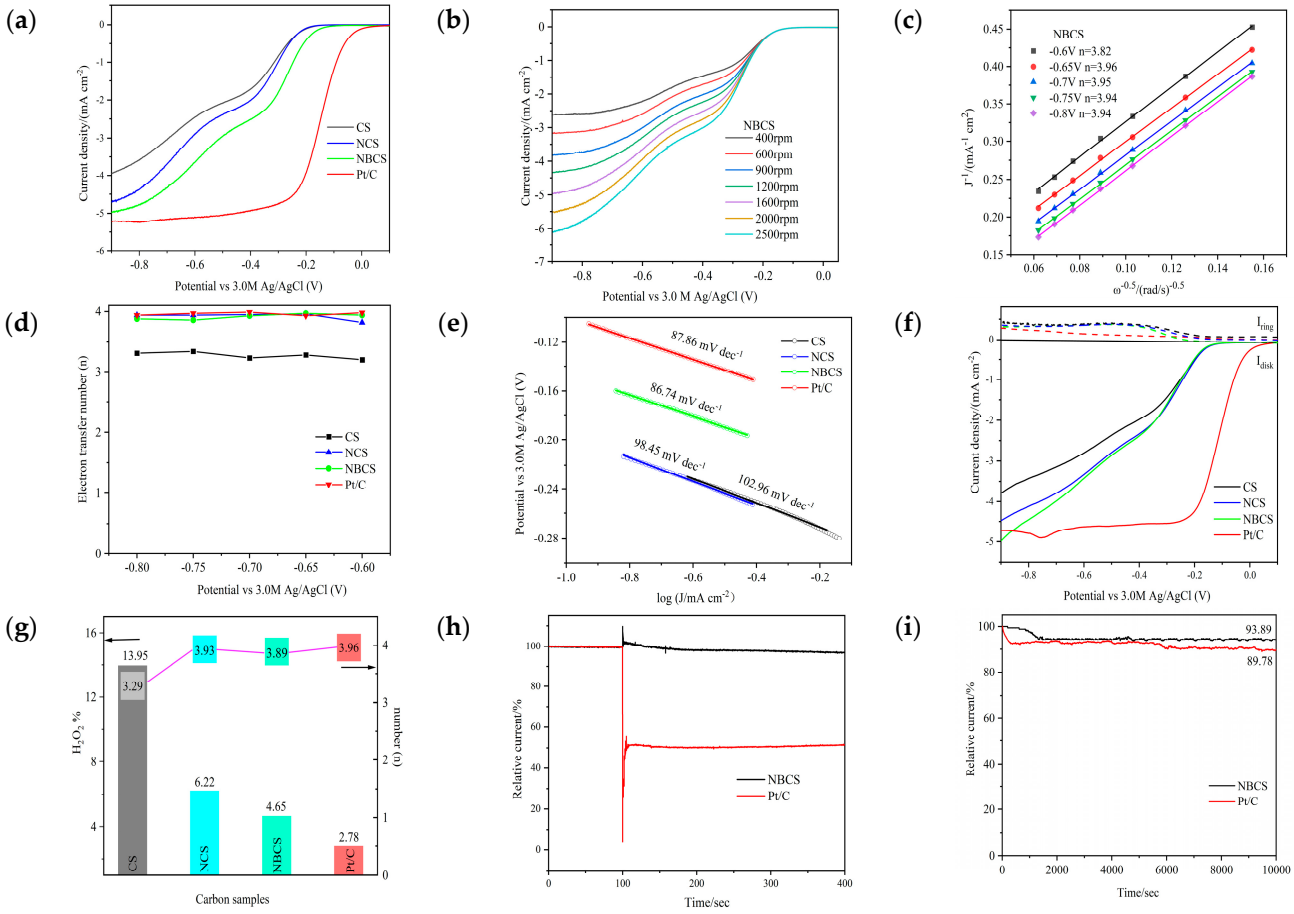

Figure 6. (**a**) LSV curves of NBCS, NCS, CS, and Pt/C; (**b**) LSV curves of NBCS at different rotational speeds; (**c**) K-L plots and the calculated number of transferred electrons of NBCS at various potentials; (**d**) number of transferred electrons of NBCS, NCS, CS, and Pt/C; (**e**) Tafel plots of NBCS, NCS, CS, and Pt/C; (**f**) LSV curves recorded on the RRDEs of NBCS, NCS, CS, and Pt/C; (**g**) yields and number of electrons transferred to H_2O_2 of NBCS, NCS, CS, and Pt/C; (**h**) methanol resistance test of NBCS and Pt/C; (**i**) stability testing of NBCS.

Table 1. Mass loading, half-wave potentials ($E_{1/2}$), and current densities of the catalysts.

Catalysts	Mass Loading (mg cm^{-2})	E_{onset} (V)	$E_{1/2}$ (V)	Current Densities (mA cm^{-2})
CS	0.414	−0.199	−0.465	−3.94
NCS	0.414	−0.203	−0.491	−4.71
NBCS	0.414	−0.148	−0.393	−4.98
Pt/C	0.204	0	−0.151	−5.21

3.3. Promotion Mechanism

Electrical conductivity showed an important influence on electron transport and reaction rate for ORR [64,65]. The measurement of electrical conductivity may help to understand the promotion mechanism of catalysts. In this work, the conductivity of the samples with pressure from 2 MPa to 20 MPa was analyzed and the results are shown in Figure 7. Generally, the electrical conductivity of all three samples increased with increasing pressure. More importantly, NBCS has the best conductivity, followed by NCS, while CS

shows the worst conductivity. This suggests that the electronic structure and energy band properties of carbon materials changed to different extents with single (the case of CS), double (the case of NCS), or triple (the case of NBCS) heteroatom doping, and the latter enhanced the conductivity, although the detailed mechanism is still under investigation. The increase in conductivity promotes electron transfer and increases the reaction rate, which ultimately improves the catalytic activity of NBCS.

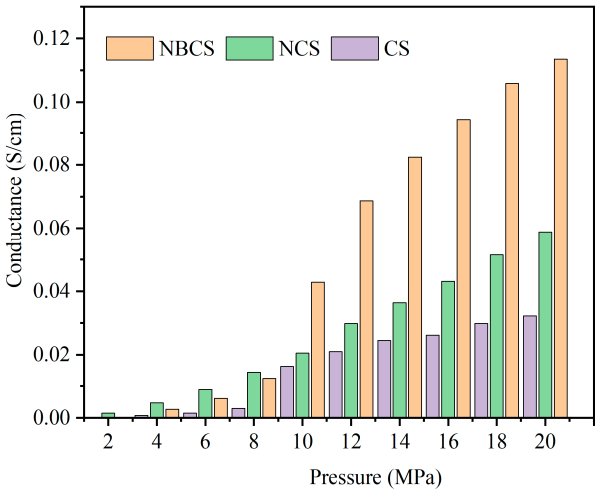

Figure 7. Conductivity of NBCS, NCS, and CS at different pressures.

4. Discussion

In summary, the triple-doped catalyst (NBCS) exhibits better ORR catalytic performance, excellent methanol resistance, and long-lasting stability compared to double-doped and single-doped (-NCS and -CS). This can be attributed to the following reasons: (1) the uniform surface distribution, large specific area, and abundant porous structure of NBCS, which help to improve the mass transfer effect; (2) the high electrical conductivity of NBCS, which accelerates the electron transfer process and is conducive to the improvement of the reaction rate; and (3) the ternary co-doping of N, B, and S on the activated carbon, which disrupts the structure of the activated carbon and alters the electronegativity around the carbon atoms, forming more active sites and enhancing the catalytic performance. The preparation of heteroatom-doped carbon-based catalysts by using the steaming process, the drastic combustion effect, the rapid reaction process, and the successful doping of heteroatoms along with a certain degree of graphitization are of great significance for the enhancement of catalytic performance. The feasibility of the cooking process is further demonstrated through continuous research and exploration.

5. Conclusions

In this work, single (CS)-, double (NCS)-, and triple (NBCS)-heteroatom-doped carbon-based catalysts were prepared using a novel "cook-off" process for oxygen reduction reaction applications. NBCS showed a uniform distribution of particles with similar sizes, while the ternary doping resulted in a micro-structure with internal defects and disorder, leading to the exposure of more active sites. Furthermore, it had a larger percentage of active pyridinic N. Therefore, it demonstrated as having the best ORR catalytic performance with the trend of CS < NCS < NBCS. Moreover, it showed much better methanol resistance and slightly higher stability than the Pt/C catalyst. The improved performance may be due to the excellent electrical conductivity of NBCS, although further investigation is required to reveal the mechanism. With further optimization and deep investigation, it may lead to the discovery of an excellent candidate to replace Pt/C.

Supplementary Materials: The following supporting information can be downloaded at: https://www.mdpi.com/article/10.3390/pr12020264/s1, experimental material. Specific values for the

RDE and RRDE parameters. Figure S1: (a) TEM images of NBCS; (b) TEM images of NCS; (c) TEM images of CS. Table S1: Different contents of raw materials in the samples. Table S2: Elemental composition of catalysts measured by XPS (at. %). Table S3: Performance of heteroatom-doped carbon materials as ORR catalysts. Refs. [66–70] are cited in the Supplementary Materials.

Author Contributions: R.Z.: investigation, data collection for measurements other than conductivity and XPS, writing—original draft. Q.L.: data collection for conductivity. M.W.: data collection for XPS. M.H.: supervision, funding acquisition, conceptualization, writing—review and editing. Z.Y.: supervision, funding acquisition, conceptualization, writing—review and editing. All authors have read and agreed to the published version of the manuscript.

Funding: This work is supported by the National Natural Science Foundation of China (NSFC) (52102256), the Natural Science Foundation of Hubei Province (2023AFB1032), Jianghan University Scientific Research Project Four New Disciplines (2022SXZX04), the Excellent Discipline Cultivation Project by JHUN (2023XKZ037), and the Graduate Research and Innovation Fund of Jianghan University 2023 (KYCXJJ202322).

Data Availability Statement: Data are contained within the article and Supplementary Materials.

Conflicts of Interest: The authors declare no conflicts of interest.

References

1. Huang, Y.; Luo, Z.; Tang, Y.; Deng, W. Analysis of the Impact of Lateral Conduit and Metal Wire Mesh on Methane Explosions. *Processes* **2023**, *11*, 3446. [CrossRef]
2. Yao, Z.; Yan, T.; Hu, M. Comparison of undergraduate chemical engineering curricula between China and America Universities based on statistical analysis. *Educ. Chem. Eng.* **2022**, *38*, 55–59. [CrossRef]
3. Fu, G.; Tang, Y.; Lee, J.-M. Recent Advances in Carbon-Based Bifunctional Oxygen Electrocatalysts for Zn-Air Batteries. *ChemElectroChem* **2018**, *5*, 1424–1434. [CrossRef]
4. Li, W.; Hu, Z.-Y.; Zhang, Z.; Wei, P.; Zhang, J.; Pu, Z.; Zhu, J.; He, D.; Mu, S.; Van Tendeloo, G. Nano-single crystal coalesced PtCu nanospheres as robust bifunctional catalyst for hydrogen evolution and oxygen reduction reactions. *J. Catal.* **2019**, *375*, 164–170. [CrossRef]
5. Gong, K.; Du, F.; Xia, Z.; Durstock, M.; Dai, L. Nitrogen-Doped Carbon Nanotube Arrays with High Electrocatalytic Activity for Oxygen Reduction. *Science* **2009**, *323*, 760–764. [CrossRef]
6. Li, Y.; Tong, Y.; Peng, F. Metal-free carbocatalysis for electrochemical oxygen reduction reaction: Activity origin and mechanism. *J. Energy Chem.* **2020**, *48*, 308–321. [CrossRef]
7. Qu, K.; Zheng, Y.; Dai, S.; Qiao, S.Z. Graphene oxide-polydopamine derived N, S-codoped carbon nanosheets as superior bifunctional electrocatalysts for oxygen reduction and evolution. *Nano Energy* **2016**, *19*, 373–381. [CrossRef]
8. Shi, Q.; Lei, Y.; Wang, Y.; Wang, H.; Jiang, L.; Yuan, H.; Fang, D.; Wang, B.; Wu, N.; Gou, Y. B, N-codoped 3D micro-/mesoporous carbon nanofibers web as efficient metal-free catalysts for oxygen reduction. *Curr. Appl. Phys.* **2015**, *15*, 1606–1614. [CrossRef]
9. Bayatsarmadi, B.; Zheng, Y.; Jaroniec, M.; Qiao, S.Z. Soft-Templating Synthesis of N-Doped Mesoporous Carbon Nanospheres for Enhanced Oxygen Reduction Reaction. *Chem. Asian J.* **2015**, *10*, 1546–1553. [CrossRef]
10. Yao, Z.; Li, L.; Liu, X.; Hui, K.N.; Shi, L.; Zhou, F.; Hu, M.; Hui, K.S. Mechanistic insights into NO-H_2 reaction over Pt/boron-doped graphene catalyst. *J. Hazard. Mater.* **2021**, *406*, 124327. [CrossRef]
11. Chen, Q.; Zhang, Z.; Zhang, R.; Hu, M.; Shi, L.; Yao, Z. Recent Progress of Non-Pt Catalysts for Oxygen Reduction Reaction in Fuel Cells. *Processes* **2023**, *11*, 361. [CrossRef]
12. Zeng, S.; Wang, S.; Zhuang, H.; Lu, B.; Li, C.; Wang, Y.; Wang, G. Fluorine-doped carbon: A metal-free electrocatalyst for oxygen reduction to peroxide. *Electrochim. Acta* **2022**, *420*, 140460. [CrossRef]
13. Sibul, R.; Kibena-Põldsepp, E.; Mäeorg, U.; Merisalu, M.; Kikas, A.; Kisand, V.; Treshchalov, A.; Sammelselg, V.; Tammeveski, K. Sulphur and nitrogen co-doped graphene-based electrocatalysts for oxygen reduction reaction in alkaline medium. *Electrochem. Commun.* **2019**, *109*, 106603. [CrossRef]
14. Wei, P.; Li, X.; He, Z.; Sun, X.; Liang, Q.; Wang, Z.; Fang, C.; Li, Q.; Yang, H.; Han, J.; et al. Porous N, B co-doped carbon nanotubes as efficient metal-free electrocatalysts for ORR and Zn-air batteries. *Chem. Eng. J.* **2021**, *422*, 130134. [CrossRef]
15. Nam, D.; Kim, J. Fe, P, N, S multidoping porous graphene material as a Bifunctional OER/ORR electrocatalytic activity for enhancing rechargeable Zn-air batteries. *Ionics* **2022**, *28*, 4719–4728. [CrossRef]
16. Li, G.-L.; Cheng, G.-C.; Chen, W.-W.; Liu, C.-D.; Yuan, L.-F.; Yang, B.-B.; Hao, C. N/S/B-doped graphitized carbon encased Fe species as a highly active and durable catalyst towards oxygen reduction reaction. *J. Colloid Interface Sci.* **2018**, *514*, 108–116. [CrossRef]
17. Li, B.; Xiang, T.; Shao, Y.; Lv, F.; Cheng, C.; Zhang, J.; Zhu, Q.; Zhang, Y.; Yang, J. Secondary-Heteroatom-Doping-Derived Synthesis of N, S Co-Doped Graphene Nanoribbons for Enhanced Oxygen Reduction Activity. *Nanomaterials* **2022**, *12*, 3306. [CrossRef]

18. Wang, Y.; Gan, R.; Zhao, S.; Ma, W.; Zhang, X.; Song, Y.; Ma, C.; Shi, J. B, N, F tri-doped lignin-derived carbon nanofibers as an efficient metal-free bifunctional electrocatalyst for ORR and OER in rechargeable liquid/solid-state Zn-air batteries. *Appl. Surf. Sci.* **2022**, *598*, 153891. [CrossRef]
19. Zhang, X.; Wang, Y.; Du, Y.; Qing, M.; Yu, F.; Tian, Z.Q.; Shen, P.K. Highly active N, S co-doped hierarchical porous carbon nanospheres from green and template-free method for super capacitors and oxygen reduction reaction. *Electrochim. Acta* **2019**, *318*, 272–280. [CrossRef]
20. Nallayagari, A.R.; Sgreccia, E.; Pasquini, L.; Vacandio, F.; Kaciulis, S.; Di Vona, M.L.; Knauth, P. Catalytic electrodes for the oxygen reduction reaction based on co-doped (B-N, Si-N, S-N) carbon quantum dots and anion exchange ionomer. *Electrochim. Acta* **2022**, *427*, 140861. [CrossRef]
21. Park, J.-E.; Jang, Y.J.; Kim, Y.J.; Song, M.-S.; Yoon, S.; Kim, D.H.; Kim, S.-J. Sulfur-doped graphene as a potential alternative metal-free electrocatalyst and Pt-catalyst supporting material for oxygen reduction reaction. *Phys. Chem. Chem. Phys.* **2014**, *16*, 103–109. [CrossRef]
22. Hu, C.; Dai, L. Multifunctional Carbon-Based Metal-Free Electrocatalysts for Simultaneous Oxygen Reduction, Oxygen Evolution, and Hydrogen Evolution. *Adv. Mater.* **2017**, *29*, 1604942. [CrossRef]
23. Oh, T.; Kim, K.; Kim, J. Controllable active sites and facile synthesis of cobalt nanoparticle embedded in nitrogen and sulfur co-doped carbon nanotubes as efficient bifunctional electrocatalysts for oxygen reduction and evolution reactions. *J. Energy Chem.* **2019**, *38*, 60–67. [CrossRef]
24. Sadegh Hassani, S.; Samiee, L.; Rashidi, A.; Ganjali, M.R. Comparative study of various preparation methods of metal-free N and S Co-doped porous graphene as an ORR catalyst in alkaline solution. *J. Chem. Sci.* **2022**, *134*, 27. [CrossRef]
25. Hu, M.; Yao, Z.; Wang, X. Graphene-Based Nanomaterials for Catalysis. *Ind. Eng. Chem. Res.* **2017**, *56*, 3477–3502. [CrossRef]
26. Liu, H.; Zhang, Y.; Li, R.; Sun, X.; Désilets, S.; Abou-Rachid, H.; Jaidann, M.; Lussier, L.-S. Structural and morphological control of aligned nitrogen-doped carbon nanotubes. *Carbon* **2010**, *48*, 1498–1507. [CrossRef]
27. Zhang, P.; Wei, J.-S.; Chen, X.-B.; Xiong, H.-M. Heteroatom-doped carbon dots based catalysts for oxygen reduction reactions. *J. Colloid Interface Sci.* **2019**, *537*, 716–724. [CrossRef]
28. Gutru, R.; Turtayeva, Z.; Xu, F.; Maranzana, G.; Thimmappa, R.; Mamlouk, M.; Desforges, A.; Vigolo, B. Recent progress in heteroatom doped carbon based electrocatalysts for oxygen reduction reaction in anion exchange membrane fuel cells. *Int. J. Hydrogen Energy* **2023**, *48*, 3593–3631. [CrossRef]
29. Feng, X.; Bai, Y.; Liu, M.; Li, Y.; Yang, H.; Wang, X.; Wu, C. Untangling the respective effects of heteroatom-doped carbon materials in batteries, supercapacitors and the ORR to design high performance materials. *Energy Environ. Sci.* **2021**, *14*, 2036–2089. [CrossRef]
30. Yang, H.; Yang, G.; Qiao, Z.; Bao, H.; Zhang, S.; Li, X.; Liu, Y. Facile Deflagration Synthesis of Hollow Carbon Nanospheres with Efficient Performance for Solar Water Evaporation. *ACS Appl. Mater. Interfaces* **2020**, *12*, 35193–35200. [CrossRef] [PubMed]
31. Yao, Z.; Hu, M.; Iqbal, Z.; Wang, X. N_8^- Polynitrogen Stabilized on Boron-Doped Graphene as Metal-Free Electrocatalysts for Oxygen Reduction Reaction. *ACS Catal.* **2020**, *10*, 160–167. [CrossRef]
32. Han, Y.; Yan, D.; Ma, Z.; Wang, Q.; Wang, X.; Li, Y.; Sun, G. Lignin-derived sulfonate base metal-free N, S co-doped carbon microspheres doped with different nitrogen sources as catalysts for oxygen reduction reactions. *Int. J. Biol. Macromol.* **2023**, *244*, 125363. [CrossRef] [PubMed]
33. Zhou, Z.; Zhang, X.; Xing, L.; Liu, J.; Kong, A.; Shan, Y. Copper-assisted thermal conversion of microporous covalent melamine-boroxine frameworks to hollow B, N-codoped carbon capsules as bifunctional metal-free electrode materials. *Electrochim. Acta* **2019**, *298*, 210–218. [CrossRef]
34. Pan, F.; Duan, Y.; Liang, A.; Zhang, J.; Li, Y. Facile Integration of Hierarchical Pores and N,P-Codoping in Carbon Networks Enables Efficient Oxygen Reduction Reaction. *Electrochim. Acta* **2017**, *238*, 375–383. [CrossRef]
35. Wang, Z.; Xu, W.; Chen, X.; Peng, Y.; Song, Y.; Lv, C.; Liu, H.; Sun, J.; Yuan, D.; Li, X.; et al. Defect-Rich Nitrogen Doped Co_3O_4/C Porous Nanocubes Enable High-Efficiency Bifunctional Oxygen Electrocatalysis. *Adv. Funct. Mater.* **2019**, *29*, 1902875. [CrossRef]
36. Zeng, X.; Wang, Z.; Meng, N.; Mccarthy, D.T.; Deletic, A.; Pan, J.H.; Zhang, X. Highly dispersed TiO_2 nanocrystals and carbon dots on reduced graphene oxide: Ternary nanocomposites for accelerated photocatalytic water disinfection. *Appl. Catal. B Environ.* **2017**, *202*, 33–41. [CrossRef]
37. Yang, L.; Shui, J.; Du, L.; Shao, Y.; Liu, J.; Dai, L.; Hu, Z. Carbon-Based Metal-Free ORR Electrocatalysts for Fuel Cells: Past, Present, and Future. *Adv. Mater.* **2019**, *31*, 1804799. [CrossRef]
38. Liu, S.; Li, G.; Gao, Y.; Xiao, Z.; Zhang, J.; Wang, Q.; Zhang, X.; Wang, L. Doping carbon nanotubes with N, S, and B for electrocatalytic oxygen reduction: A systematic investigation on single, double, and triple doped modes. *Catal. Sci. Technol.* **2017**, *7*, 4007–4016. [CrossRef]
39. Dong, F.; Cai, Y.; Liu, C.; Liu, J.; Qiao, J. Heteroatom (B, N and P) doped porous graphene foams for efficient oxygen reduction reaction electrocatalysis. *Int. J. Hydrogen Energy* **2018**, *43*, 12661–12670. [CrossRef]
40. Wu, M.; Wang, Y.; Wei, Z.; Wang, L.; Zhuo, M.; Zhang, J.; Han, X.; Ma, J. Ternary doped porous carbon nanofibers with excellent ORR and OER performance for zinc–air batteries. *J. Mater. Chem. A* **2018**, *6*, 10918–10925. [CrossRef]
41. Jiao, Y.; Zheng, Y.; Jaroniec, M.; Qiao, S.Z. Origin of the Electrocatalytic Oxygen Reduction Activity of Graphene-Based Catalysts: A Roadmap to Achieve the Best Performance. *J. Am. Chem. Soc.* **2014**, *136*, 4394–4403. [CrossRef]

42. Jin, J.; Pan, F.; Jiang, L.; Fu, X.; Liang, A.; Wei, Z.; Zhang, J.; Sun, G. Catalyst-Free Synthesis of Crumpled Boron and Nitrogen Co-Doped Graphite Layers with Tunable Bond Structure for Oxygen Reduction Reaction. *ACS Nano* **2014**, *8*, 3313–3321. [CrossRef] [PubMed]
43. Li, D.; Ren, B.; Jin, Q.; Cui, H.; Wang, C. Nitrogen-doped, oxygen-functionalized, edge- and defect-rich vertically aligned graphene for highly enhanced oxygen evolution reaction. *J. Mater. Chem. A* **2018**, *6*, 2176–2183. [CrossRef]
44. Liu, T.; Guo, Y.-F.; Yan, Y.-M.; Wang, F.; Deng, C.; Rooney, D.; Sun, K.-N. CoO nanoparticles embedded in three-dimensional nitrogen/sulfur co-doped carbon nanofiber networks as a bifunctional catalyst for oxygen reduction/evolution reactions. *Carbon* **2016**, *106*, 84–92. [CrossRef]
45. Qu, K.; Zheng, Y.; Jiao, Y.; Zhang, X.; Dai, S.; Qiao, S.-Z. Polydopamine-Inspired, Dual Heteroatom-Doped Carbon Nanotubes for Highly Efficient Overall Water Splitting. *Adv. Energy Mater.* **2017**, *7*, 1602068. [CrossRef]
46. Wang, X.; Sun, G.; Routh, P.; Kim, D.-H.; Huang, W.; Chen, P. Heteroatom-doped graphene materials: Syntheses, properties and applications. *Chem. Soc. Rev.* **2014**, *43*, 7067–7098. [CrossRef]
47. Patel, M.A.; Luo, F.; Savaram, K.; Kucheryavy, P.; Xie, Q.; Flach, C.; Mendelsohn, R.; Garfunkel, E.; Lockard, J.V.; He, H. P and S dual-doped graphitic porous carbon for aerobic oxidation reactions: Enhanced catalytic activity and catalytic sites. *Carbon* **2017**, *114*, 383–392. [CrossRef]
48. You, C.; Liao, S.; Li, H.; Hou, S.; Peng, H.; Zeng, X.; Liu, F.; Zheng, R.; Fu, Z.; Li, Y. Uniform nitrogen and sulfur co-doped carbon nanospheres as catalysts for the oxygen reduction reaction. *Carbon* **2014**, *69*, 294–301. [CrossRef]
49. Inagaki, M.; Toyoda, M.; Soneda, Y.; Morishita, T. Nitrogen-doped carbon materials. *Carbon* **2018**, *132*, 104–140. [CrossRef]
50. Zhou, Y.; Sun, Y.; Wang, H.; Zhu, C.; Gao, J.; Wu, D.; Huang, H.; Liu, Y.; Kang, Z. A nitrogen and boron co-doped metal-free carbon electrocatalyst for an efficient oxygen reduction reaction. *Inorg. Chem. Front.* **2018**, *5*, 2985–2991. [CrossRef]
51. Shin, D.; Jeong, B.; Mun, B.S.; Jeon, H.; Shin, H.-J.; Baik, J.; Lee, J. On the Origin of Electrocatalytic Oxygen Reduction Reaction on Electrospun Nitrogen-Carbon Species. *J. Phys. Chem. C* **2013**, *117*, 11619–11624. [CrossRef]
52. Zhu, J.; Zhou, H.; Zhang, C.; Zhang, J.; Mu, S. Dual active nitrogen doped hierarchical porous hollow carbon nanospheres as an oxygen reduction electrocatalyst for zinc-air batteries. *Nanoscale* **2017**, *9*, 13257–13263. [CrossRef] [PubMed]
53. Zhang, C.; Selch, D.; Xie, Z.; Roberts, C.; Cooper, H.; Chen, G. Object-based benthic habitat mapping in the Florida Keys from hyperspectral imagery. *Estuar. Coast. Shelf Sci.* **2013**, *134*, 88–97. [CrossRef]
54. Yu, J.; Wang, C.; Yuan, W.; Shen, Y.; Xie, A. B, N Co-Doped Three-Dimensional Carbon Aerogels with Excellent Electrochemical Performance for the Oxygen Reduction Reaction. *Chem. A Eur. J.* **2019**, *25*, 2877–2883. [CrossRef]
55. Kodithuwakku, U.S.; Wanninayake, N.; Thomas, M.P.; Guiton, B.S.; Kim, D.Y. Unlocking efficiency in oxygen reduction reaction: Synergistic edge dopants of nitrogen and boron in carbon nano onions. *Electrochim. Acta* **2023**, *471*, 143365. [CrossRef]
56. Wang, W.; Chen, J.-Q.; Tao, Y.-R.; Zhu, S.-N.; Zhang, Y.-X.; Wu, X.-C. Flowerlike Ag-Supported Ce-Doped Mn_3O_4 Nanosheet Heterostructure for a Highly Efficient Oxygen Reduction Reaction: Roles of Metal Oxides in Ag Surface States. *ACS Catal.* **2019**, *9*, 3498–3510. [CrossRef]
57. Jin, H.; Huang, H.; He, Y.; Feng, X.; Wang, S.; Dai, L.; Wang, J. Graphene Quantum Dots Supported by Graphene Nanoribbons with Ultrahigh Electrocatalytic Performance for Oxygen Reduction. *J. Am. Chem. Soc.* **2015**, *137*, 7588–7591. [CrossRef]
58. Li, Y.; Zhao, Y.; Cheng, H.; Hu, Y.; Shi, G.; Dai, L.; Qu, L. Nitrogen-Doped Graphene Quantum Dots with Oxygen-Rich Functional Groups. *J. Am. Chem. Soc.* **2012**, *134*, 15–18. [CrossRef]
59. Wang, Y.; Liu, H.; Wang, K.; Song, S.; Tsiakaras, P. 3D interconnected hierarchically porous N-doped carbon with NH_3 activation for efficient oxygen reduction reaction. *Appl. Catal. B Environ.* **2017**, *210*, 57–66. [CrossRef]
60. Liu, J.-N.; Li, B.-Q.; Zhao, C.-X.; Yu, J.; Zhang, Q. A Composite Bifunctional Oxygen Electrocatalyst for High-Performance Rechargeable Zinc-Air Batteries. *ChemSusChem* **2020**, *13*, 1529–1536. [CrossRef]
61. Cao, S.; Shang, W.; Li, G.-L.; Lu, Z.-F.; Wang, X.; Yan, Y.; Hao, C.; Wang, S.; Sun, G. Defect-rich and metal-free N, S co-doped 3D interconnected mesoporous carbon material as an advanced electrocatalyst towards oxygen reduction reaction. *Carbon* **2021**, *184*, 127–135. [CrossRef]
62. Duraisamy, V.; Senthil Kumar, S.M. N and P dual heteroatom doped mesoporous hollow carbon as an efficient oxygen reduction reaction catalyst in alkaline electrolyte. *Int. J. Hydrogen Energy* **2022**, *47*, 17992–18006. [CrossRef]
63. Kim, M.; Firestein, K.L.; Fernando, J.F.S.; Xu, X.; Lim, H.; Golberg, D.V.; Na, J.; Kim, J.; Nara, H.; Tang, J.; et al. Strategic design of Fe and N co-doped hierarchically porous carbon as superior ORR catalyst: From the perspective of nanoarchitectonics. *Chem. Sci.* **2022**, *13*, 10836–10845. [CrossRef]
64. Zhang, W.; Pu, W.; Qu, Y.; Yang, H.; Liu, Y. Facile synthesis of ultrathin S-N co-doped carbon nanosheet as ORR electrocatalysts for application in sustainable zinc-air battery. *Electrochim. Acta* **2023**, *462*, 142800. [CrossRef]
65. Huang, X.; Wang, Y.; Li, W.; Hou, Y. Noble metal-free catalysts for oxygen reduction reaction. *Sci. China Chem.* **2017**, *60*, 1494–1507. [CrossRef]
66. Zhang, M.; Dai, L. Carbon nanomaterials as metal-free catalysts in next generation fuel cells. *Nano Energy* **2012**, *1*, 514–517. [CrossRef]
67. Zhao, L.; Sui, X.-L.; Li, J.-Z.; Zhang, J.-J.; Zhang, L.-M.; Huang, G.-S.; Wang, Z.-B. Supramolecular assembly promoted synthesis of three-dimensional nitrogen doped graphene frameworks as efficient electrocatalyst for oxygen reduction reaction and methanol electrooxidation. *Appl. Catal. B Environ.* **2018**, *231*, 224–233. [CrossRef]

68. Meng, Y.; Voiry, D.; Goswami, A.; Zou, X.; Huang, X.; Chhowalla, M.; Liu, Z.; Asefa, T. N-, O-, and S-Tridoped Nanoporous Carbons as Selective Catalysts for Oxygen Reduction and Alcohol Oxidation Reactions. *J. Am. Chem. Soc.* **2014**, *136*, 13554–13557. [CrossRef]
69. Chang, F.; Su, P.; Guharoy, U.; Ye, R.; Ma, Y.; Zheng, H.; Jia, Y.; Liu, J. Edge-enriched N, S co-doped hierarchical porous carbon for oxygen reduction reaction. *Chin. Chem. Lett.* **2023**, *34*, 107462. [CrossRef]
70. Palm, I.; Kibena-Põldsepp, E.; Mooste, M.; Kozlova, J.; Käärik, M.; Kikas, A.; Treshchalov, A.; Leis, J.; Kisand, V.; Tamm, A.; et al. Nitrogen and sulphur co-doped carbon-based composites as electrocatalysts for the anion-exchange membrane fuel cell cathode. *Int. J. Hydrogen Energy* **2024**, *55*, 805–814. [CrossRef]